Journal of Power Sources 242 (2013) 357–364

Contents lists available at SciVerse ScienceDirect

Journal of Power Sources

journal homepage: www.elsevier.com/locate/jpowsour

Crystal modification of iron oxide scale by potassium addition and its application to lithium-ion battery anodes

Dong-Won Jung [a], Sang-Wook Han [a], Byung-Seon Kong [b], Eun-Suok Oh [a,*]

[a] School of Chemical Engineering, University of Ulsan, Ulsan 680-749, Republic of Korea
[b] KCC Central Research Institute, 83 Mabook-Dong, Giheung-Gu, Yongin, Kyunggi-Do 446-912, Republic of Korea

HIGHLIGHTS

- We suggest a simple method to reuse iron oxide scale (IOS) as anode materials in LIBs.
- The IOSs are successfully modified by KOH via a thermal diffusion process.
- KOH-treated IOS exhibits excellent cyclic capability and high reversible capacity.
- This improved performance is attributed to the unique structure of $KFeO_2$ crystals.

GRAPHICAL ABSTRACT

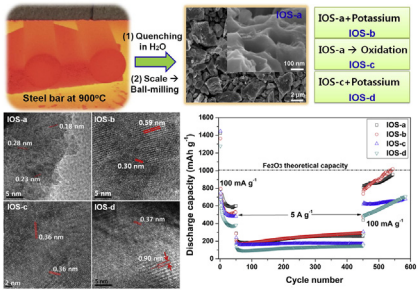

ARTICLE INFO

Article history:
Received 16 April 2013
Received in revised form
20 May 2013
Accepted 21 May 2013
Available online 4 June 2013

Keywords:
Iron oxide scale
Potassium iron oxide
Anode active materials
Lithium-ion battery
Electrochemical characterization

ABSTRACT

This paper proposes a valuable method to reuse the iron oxide scale (IOS) often produced in the steel industry as an anode active material in lithium-ion batteries (LIBs). The IOS samples are prepared via quenching of carbon steel and simple oxidation at a high temperature with or without sequential treatment by potassium hydroxide. Morphological and physical characterizations confirm the formation of a lamellar structure of orthorhombic $KFeO_2$ with a high degree of crystallinity in the potassium-added IOSs. Additionally, the potassium addition decreases the particle size of the crystals and increases the d-spacing between crystal layers. Electrochemical performance tests show that the discharge capacities of the IOS samples monotonically increased with increasing number of charge/discharge cycles regardless of the existence of potassium. In addition, the rate of increase is larger in the potassium-added IOS samples containing the lamellar $KFeO_2$ structure. Consequently, after prolonged cycling (more than 500 cycles), the potassium-added IOS sample retains a discharge capacity of 1020 mAh g^{-1} with good cycling stability, while the IOS quenched sample only exhibits a capacity of 956 mAh g^{-1}. This result is attributed to the unique structure of the $KFeO_2$ crystals formed in the potassium-added IOS particles.

1. Introduction

Carbon steel is an alloy containing iron and carbon in which the carbon content is normally in the range of 0.2–2.1% by weight. Carbon steel is generally heat-treated to achieve suitable physical and mechanical properties as it responds rapidly to heating or cooling. Quenching is a rapid cooling process which produces steel with hard and strong microstructures and forms numerous iron oxide scales (IOSs) on the surface of the steel including magnetite (Fe_3O_4), hematite (Fe_2O_3), and wüstite (FeO). Most of the IOS is remelted to produce more steel, but this process requires large amounts of coke, limestone, and fossil fuels. Recently, Fe_3O_4 and Fe_2O_3 have attracted much attention as anode materials for lithium-ion batteries (LIBs) due to their high theoretical lithium

* Corresponding author. Tel.: +82 52 259 2783; fax: +82 52 259 1689.
E-mail address: esoh1@ulsan.ac.kr (E.-S. Oh).

0378-7753/$ – see front matter © 2013 Elsevier B.V. All rights reserved.
http://dx.doi.org/10.1016/j.jpowsour.2013.05.091

storage capacities above 900 mAh g^{-1} [1–4]. Unfortunately, these materials experience large volumetric changes during charge/discharge processes with lithium ions, ultimately leading to rapid degradation of their anodic performance. This behavior is very dependent on the treatment of the IOSs.

In this study, we evaluated the anodic performance of IOSs pretreated by quenching and severe oxidation and propose a technique involving potassium doping to improve their anodic performance. Gleitzer et al. [5,6] reported that potassium ions trapped in the lattices of iron oxides accelerated oxygen exchange and increased the mobility of oxygen ions, resulting in smaller iron oxide particles with porous and locally-distorted surfaces. From the perspective of anodic performance, small and porous active particles give rise to a large surface area and short path lengths for electronic and ionic transports, resulting in a higher electrode/electrolyte contact area and quick charge/discharge current rates [7–9]. Additionally, the significant change in volume can be alleviated by using nano-sized active materials, which results in stable and improved cyclability over long-term use [1]. It is also known that an electrode containing potassium salt can improve LIB rate performance without any harmful effects such as electrode corrosion [10]. The positive effects of the addition of potassium ions on the anodic performance of IOS were thoroughly investigated in this study.

2. Experimental

Carbon steel (S45C, JIS G4051) was heated to 900 °C in air and rapidly quenched in de-ionized water at room temperature. The IOS collected through the quenching process was dried at 80 °C and separated from impurities by magnetic filtration. Three grams of the IOS was placed in a steel jar containing steel beads (10 mm: 3 EA, 5 mm: 12 EA) and was ball-milled using a vertical mini-mill (Pulverisette 23, Fritsch Co.) at 50 Hz for 20 min to reduce the particle size. The resulting material is referred to as IOS-a. The IOS-a was ultra-sonicated in potassium hydroxide (KOH) solution (30%, Alfa–Aesar Co.) for 10 min and dried in a convection oven at 80 °C overnight. The weight ratio of KOH to IOS-a was 1. The resulting material was calcined at 600 °C in a N_2 atmosphere for 5 h. The material produced is referred to as IOS-b. Additionally, a more oxidized sample, IOS-c, was synthesized by heating IOS-a at 570 °C in an air atmosphere for 3 h. This oxide was also used to produce potassium-doped and more oxidized iron oxide, IOS-d, by applying the same procedure as that used to generate IOS-b.

The crystal structures and phase composition of the treated IOS samples were determined using an X-ray diffractometer (XRD, Rigaku, RAD-3C) with a CuKα (λ = 1.541 Å) source. Morphological characterizations of the treated IOS samples were characterized using a scanning electron microscope (SEM, Carl Zeiss, Supra40) with a field emission gun, and a transmission electron microscope (TEM, JEOL, JEM-2100F).

The electrochemical characteristics of the samples as LIB anodes were evaluated in CR2016 coin cells with lithium metal as a counter and reference electrode. The working electrodes were composed of 50 wt.% treated IOS, 30 wt.% super-P as an electrically-conductive additive, and 20 wt.% polyvinylidene fluoride (Solef 5130, Belgium) as a binder. Their loading densities were 1.3 ± 0.1 mg cm^{-2}. As an electrolyte, 1 M $LiPF_6$ (Panaxetec Co., Korea) dissolved in a 1:1:1 (v/v/v) mixture of ethylene carbonate, dimethyl carbonate, and ethyl methyl carbonate was used. The coin cells were galvanostatically charged to 3 V and discharged to 5 mV at various current densities in a battery test system (PNE solution BCP50). Additionally, cyclic voltammetry (CV, Biologis VSP) and electrochemical impedance spectroscopy (EIS) were performed from 3 V to 0 V at a potential sweep rate of 0.5 mV s^{-1} and at a frequency range of 0.01 Hz–100 kHz, respectively.

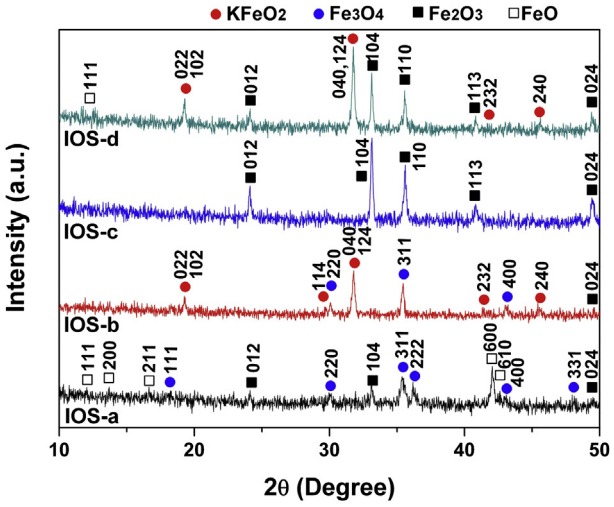

Fig. 1. XRD peaks of the treated IOS samples: IOS-a (quenching), IOS-b (quenching and potassium addition), IOS-c (quenching and oxidation), and IOS-d (quenching, oxidation, and potassium addition).

Some of the coin cells charged/discharged more than 300 times were disassembled in an argon-filled glove box and their anode materials were washed with dimethyl carbonated and stripped away from the copper foil. The remaining electrolyte and organic matters in the materials were eliminated by ultrasonication in a 1:9 (v/v) mixture of de-ionized water and ethanol for 20 min. The particles collected via filter paper were dried in a vacuum oven at 80 °C for 30 min and their crystal structures were investigated using XRD and TEM analyses.

3. Results and discussion

The crystal structures of the treated IOS samples were characterized by their XRD peaks, as shown in Fig. 1. The XRD pattern of IOS-a indicates that various iron oxide crystals such as Fe_3O_4 (JCPDS No. 87-2334), Fe_2O_3 (JCPDS No. 87-1165), and FeO (JCPDS No. 87-2316) were formed during the quenching process. As seen from the XRD peaks of the IOS-b sample in Fig. 1, the KOH treatment transforms some of iron oxides, especially Fe_2O_3, into an orthorhombic $KFeO_2$ compound (JCPDS No. 83-2153) with a high crystallinity. The IOS-c sample produced by an additional oxidation step showed a higher crystallinity than the IOS-a sample, and most of the XRD peaks are assigned to rhombohedral Fe_2O_3, clearly indicating that both Fe_3O_4 and FeO phases are transformed into a relatively high oxidation form of iron, Fe_2O_3. Thus, the XRD spectra of the IOS-d sample show peaks that can be assigned to the mixture of $KFeO_2$ and Fe_2O_3 only. Relative quantitative percentages of each crystalline phase in the IOS samples were determined from the comparison among integrated XRD peak areas and were listed in Table 1.

Table 1
Particle size and quantitative percentage of IOS samples estimated by the XRD peaks.

Samples	Quantitative percentage of crystalline phase (%)				Mean particle size (nm)
	$KFeO_2$	Fe_3O_4	Fe_2O_3	FeO	
IOS-a	0	43.9	18.9	37.2	64.8
IOS-b	50.8	44.0	5.2	0	23.3
IOS-c	0	11.0	89.0	0	53.2
IOS-d	41.3	0	55.3	3.4	49.1

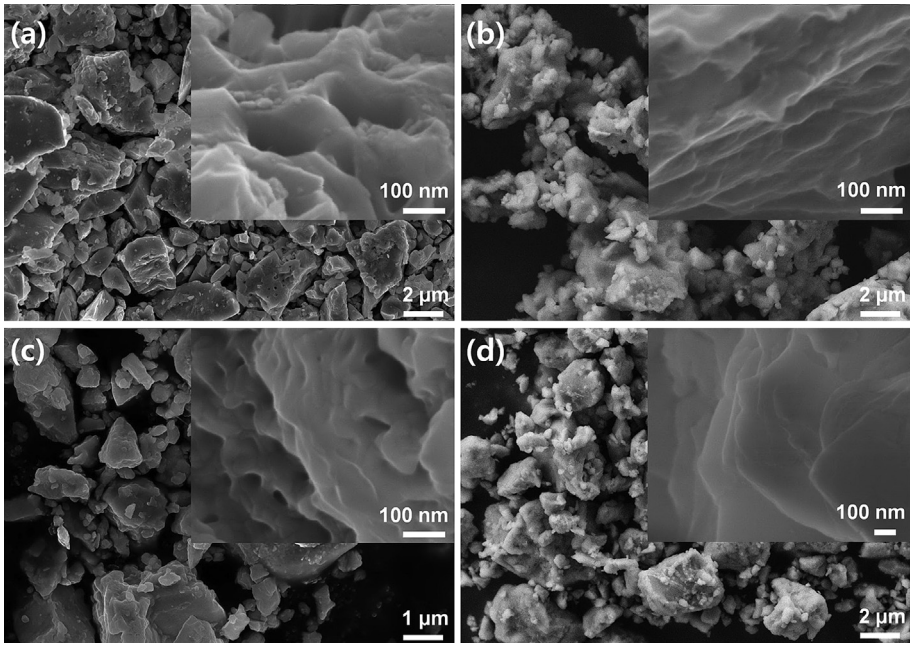

Fig. 2. SEM images of the (a) IOS-a, (b) IOS-b, (c) IOS-c, and (d) IOS-d samples. The insets are magnified images.

Based on the Scherrer equation [11], the calculated mean crystallite sizes of the IOS-a, IOS-b, IOS-c, and IOS-d particles are 64.8 nm, 23.3 nm, 53.2 nm, and 49.1 nm, respectively, as shown also in Table 1. The treatment with KOH makes the iron oxide particles smaller, especially in the low crystalline sample, IOS-a, and makes the crystal d-spacing broader due to the phase transformation from iron oxides to $KFeO_2$. For instance, the d-spacing in the (022) $KFeO_2$ crystals corresponding to $2\theta = 19.3^\circ$ is 4.59 Å, which is larger than

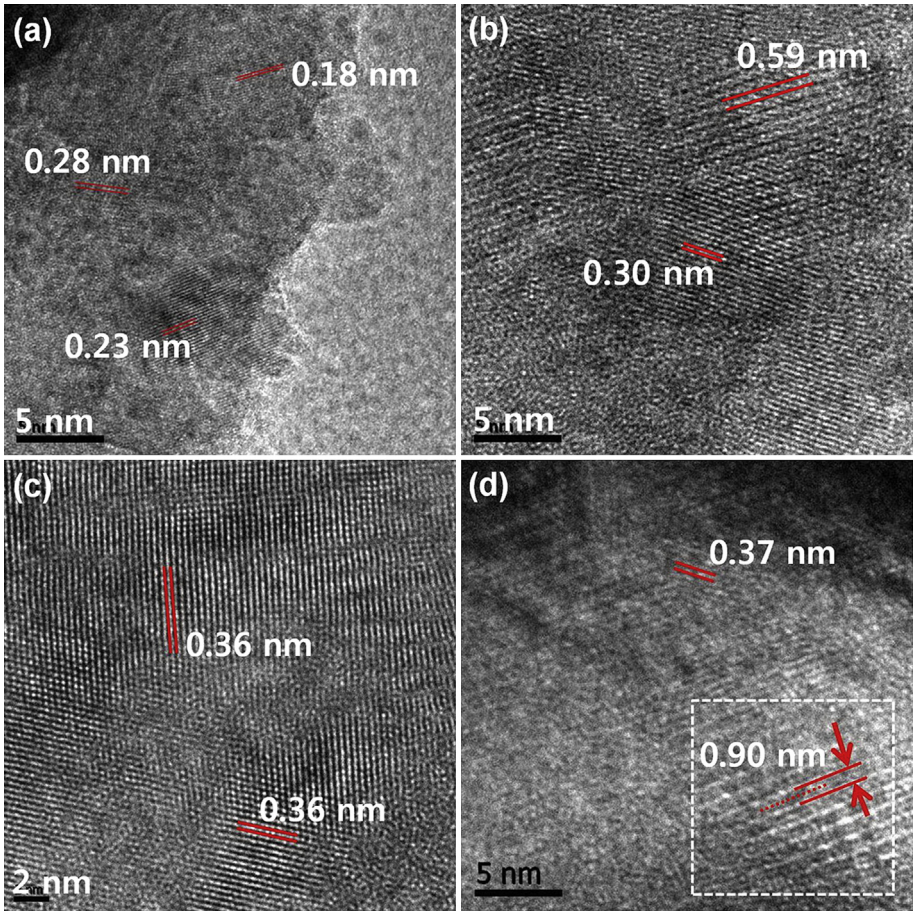

Fig. 3. TEM images of the (a) IOS-a, (b) IOS-b, (c) IOS-c, and (d) IOS-d samples.

the d-spacings in most iron oxides. This d-spacing is even larger than the typical van der Waals gap of graphite (3.35 Å). This can be clearly seen from the SEM and TEM images of the morphology displayed in Figs. 2 and 3, respectively.

The potassium-added IOS-b and IOS-d samples shown in Fig. 2b and d, respectively, have smaller particles than the iron oxide samples without potassium addition, IOS-a and IOS-c, shown in Fig. 2a and c, respectively. Additionally, fine pores in the IOS-a and IOS-c samples generated by gas emission during quenching in water are not observed in the IOS-b and IOS-d samples. As seen in Fig. 1, the KOH treatment forms new crystalline particles in iron oxides due to the reconstruction of iron, oxygen, and potassium atoms, and thus breaks the porous structure. Based on experiments done to investigate the role of potassium in FeO, Gleitzer et al. [5,6] observed that potassium ions diffused into FeO lattices and accelerated oxygen exchange in iron oxides, leading to smaller iron oxides and surface reformation. As shown in the insets of Fig. 2b and d, lamellar structures were also observed after the KOH treatment. These structures are likely the high-crystallinity $KFeO_2$ (040) crystal planes shown in the XRD analysis results in Fig. 1. Recently, Wu et al. [12] identified the presence of two-dimensional layers containing alkali metals such as sodium and potassium when the metals were intercalated into the crystal planes of iron oxides.

TEM observation of the four samples was also carried out, and the images are displayed in Fig. 3. Based on the JCPDS data of Fe_3O_4 (No. 87-2334) and Fe_2O_3 (No. 87-1165), d-spacings of 0.28, 0.23, and 0.18 nm can be assigned to Fe_2O_3 (104), Fe_3O_4 (222), and Fe_2O_3 (024) crystal planes, respectively, from the TEM image of the as-prepared IOS-a particles shown in Fig. 3a. These d-spacings increased after the KOH treatment due to the formation of new $KFeO_2$ crystals, as shown in Fig. 3b. The $KFeO_2$ (020) crystal possesses an orthorhombic structure in which potassium layers are formed between Fe–Fe and O–O planes with lattice constants of $a = 5.60$ Å, $b = 11.24$ Å, and $c = 15.91$ Å along with a space symmetry of *Pbca* (JCPDS No. 83-2153). Therefore, the formation of $KFeO_2$ phases leads to an increase in the d-spacing by as much as 0.59 nm. In addition, 0.30 nm d-spacing of the (220) plane of face-centered cubic Fe_3O_4 with a lattice constant of a = 8.40 Å and $Fd\bar{3}m$ space symmetry (JCPDS No. 87-2334) is also observed in the IOS-b sample. Meanwhile, as expected from the XRD results, the TEM image of the IOS-c sample in Fig. 3c shows highly crystalline structures that can be attributed to Fe_2O_3 crystals oxidized from various iron oxides. The d-spacing increased to 0.36 nm as a result of the oxidation, which corresponded to the interlayer distance of the Fe_2O_3 (012) planes. Subsequent KOH treatment transforms some of the Fe_2O_3 phases to $KFeO_2$ due to the diffusion of potassium ions into Fe_2O_3 lattices and/or the removal of oxygen anions with potassium cations from Fe_2O_3 lattices. Therefore, the d-spacings of 0.37 nm and 0.90 nm in Fig. 3d correspond to those of the Fe_2O_3 (012) and $KFeO_2$ (022) planes, respectively. In particular, the disappearance of part of the atomic layers in the (022) plane, which is the so-called line defect, was observed (square in Fig. 3d), which is evidence that potassium ions accelerate oxygen removal in iron oxides [5]. These defects may provide places for lithium-ion insertion/desertion, resulting in higher LIB capacity.

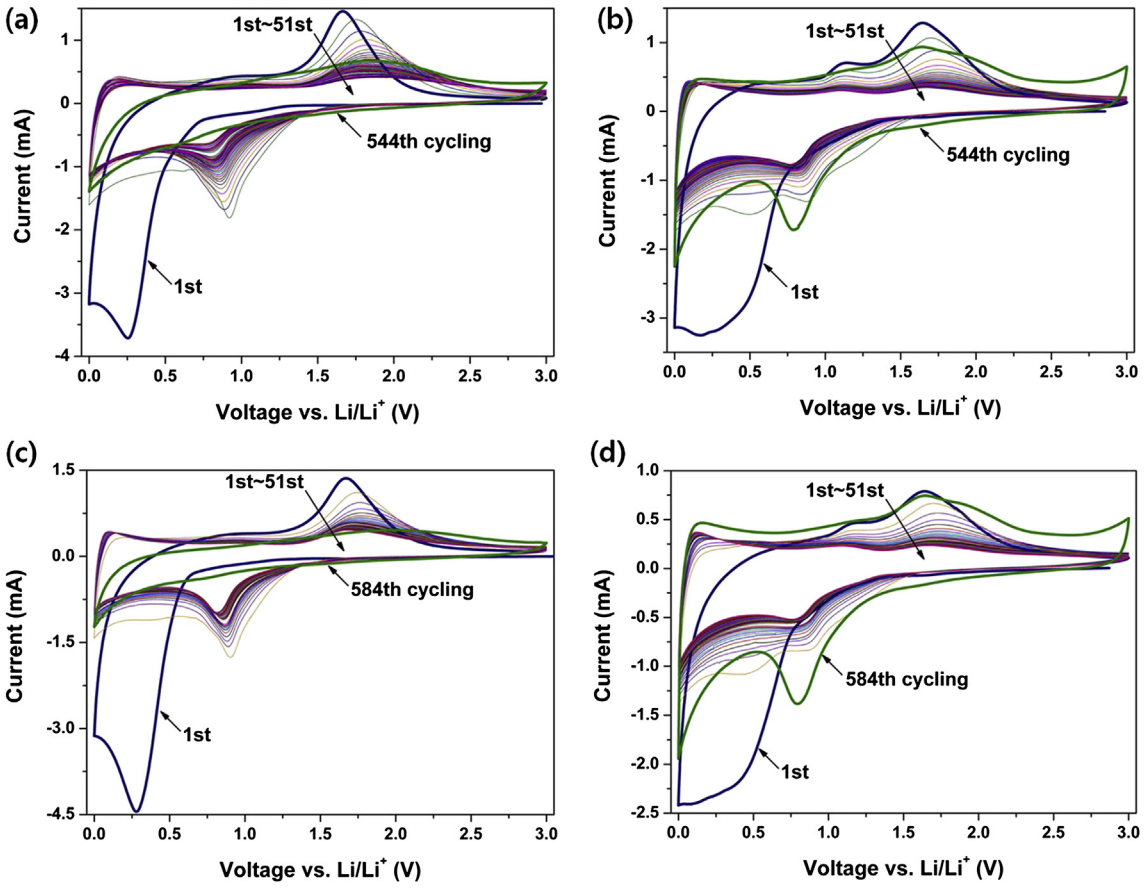

Fig. 4. Repeated cyclic voltammograms of (a) IOS-a, (b) IOS-b, (c) IOS-c, and (d) IOS-d electrodes subjected to 51 cycles. The cyclic voltammograms of the electrodes cycled extensively (544 times for IOS-a and IOS-b, 584 times for IOS-c and IOS-d) are displayed as green curves. (For interpretation of the references to colour in this figure legend, the reader is referred to the web version of this article.)

The electrochemical characteristics of the materials were analyzed by conducting CV, EIS, and cyclic performance tests. The electrochemical reactions were identified by the CV profiles shown in Fig. 4. In the first cycles of all samples, there are high intensity cathodic current flows under 0.8 V, which can be ascribed to the formation of a solid electrolyte interface (SEI) film. The cycled CV profiles can be divided into two parts: conversion and intercalation/deintercalation reactions. The strong cathodic and anodic peaks appearing around 0.9 and 1.7 V, respectively, are assigned to reversible conversion reactions between Fe^0 and Fe^{2+}/Fe^{3+} ions [4,13,14]. The other anodic peak at 1.12 V observed only in the potassium-added samples is also related to these conversion reactions of the oxidation of either potassium or iron atoms. In general, the conversion reactions are accompanied by a significant volume change, lead to extremely high stresses, and ultimately pulverize active materials over the course of their use. As a result of these phenomena, parts of the active materials are electrically isolated and are inactive, and thus the current generated by the conversion reaction continuously decreases with an increasing number of cycles, as shown in Fig. 4.

Similar to a graphite electrode, the cathodic and anodic peaks around 0 V in Fig. 4 are attributed to reversible intercalation/deintercalation reactions of lithium ions into/out of layered iron oxide structures. After prolonged cycling (more than 500 cycles), these peaks shrink or disappear in the IOS-a and IOS-c samples, indicating that the layered structures collapse. On the other hand, the potassium-added samples, IOS-b and IOS-d, still show peaks after extensive cycling and the intensities of the peaks even increase. In addition, the peaks corresponding to the conversion reactions are restored in the potassium-added samples, whereas they are not restored in the samples without added potassium. Therefore, it is thought that potassium doping contributes to maintaining the lamellar structures shown in Fig. 2b and d and enhancing the electrical contact due to the rearrangement of iron oxides during the repeated charge and discharge processes.

The electrochemical performances of the four samples were evaluated through charge/discharge tests at various current rates. As shown in Fig. 5a, the initial discharge capacities of the IOS-a, IOS-b, IOS-c, and IOS-d samples at 100 mA g^{-1} were 1425, 1363, 1448, and 1276 mAh g^{-1}, respectively, which are similar to previously-obtained results of nano-sized Fe_2O_3 and Fe_3O_4 anode materials [4,14,15]. The Coulombic efficiencies of all four samples in the first cycle were in the range of 44–48%. The high initial capacities significantly decreased at the second cycle due to irreversible reactions, including the formation of SEI layers [16]. The discharge capacities monotonically increased with increasing cycle number after approximately 100 cycles, regardless of the sample and the current rate, which is unusual behavior. The discharge capacities of the potassium-added samples increased faster than those of the samples without potassium. The increase may be due to internal structural changes in the electrodes caused by both the rearrangement of metal particles with conversion reactions and the formation of a polymeric gel-like film [17–19]. Grugeon et al. [17] proposed that nano-sized 3d-transition metals (Co, Ni, Cu, or Fe) converted from their oxides reversibly react with liquid electrolyte and form a gel-like polymer film at the surface of the metals, and that the reversible formation and dissolution of the polymer film leads to overcapacities more than the theoretical capacities of 3d-transition metal oxides. At the 500th cycles, the Coulombic efficiencies of the four samples were approximately 81–84%. These low Coulombic efficiencies are also attributed to the super-P carbon black used as a conductive agent. Recently, Gnanamuthu and Lee [20] reported that the Coulombic efficiency of super-P at the 20th cycle was approximately 84%.

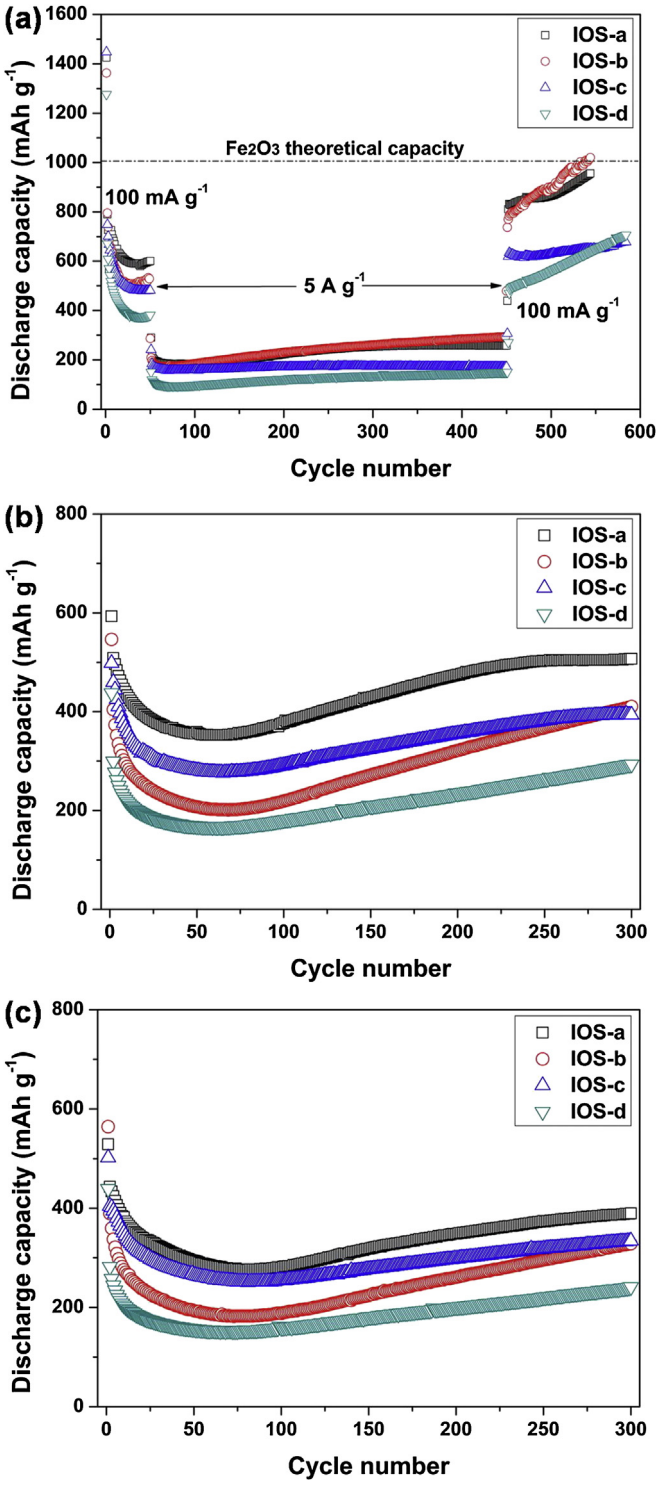

Fig. 5. Long-term cycling performance of the four IOS samples at current densities of (a) 0.1, 5, and 0.1 A g^{-1}, (b) 1 A g^{-1}, and (c) 2 A g^{-1}.

Fig. 6 displays the charge/discharge profiles of the IOS electrodes at the 1st, 2nd, 3rd, 500th, and 544th or 584th cycle at a current density of 100 mA g^{-1}. The long plateaus of the first discharge profiles occurring at approximately 0.8 V correspond to the reduction of Fe^{2+}/Fe^{3+} ions to Fe^0 by the conversion reactions [21]. This is followed by a smooth voltage drop attributed to the most part irreversible decomposition of the electrolyte to form SEI layers. Compared to the samples without potassium addition, the

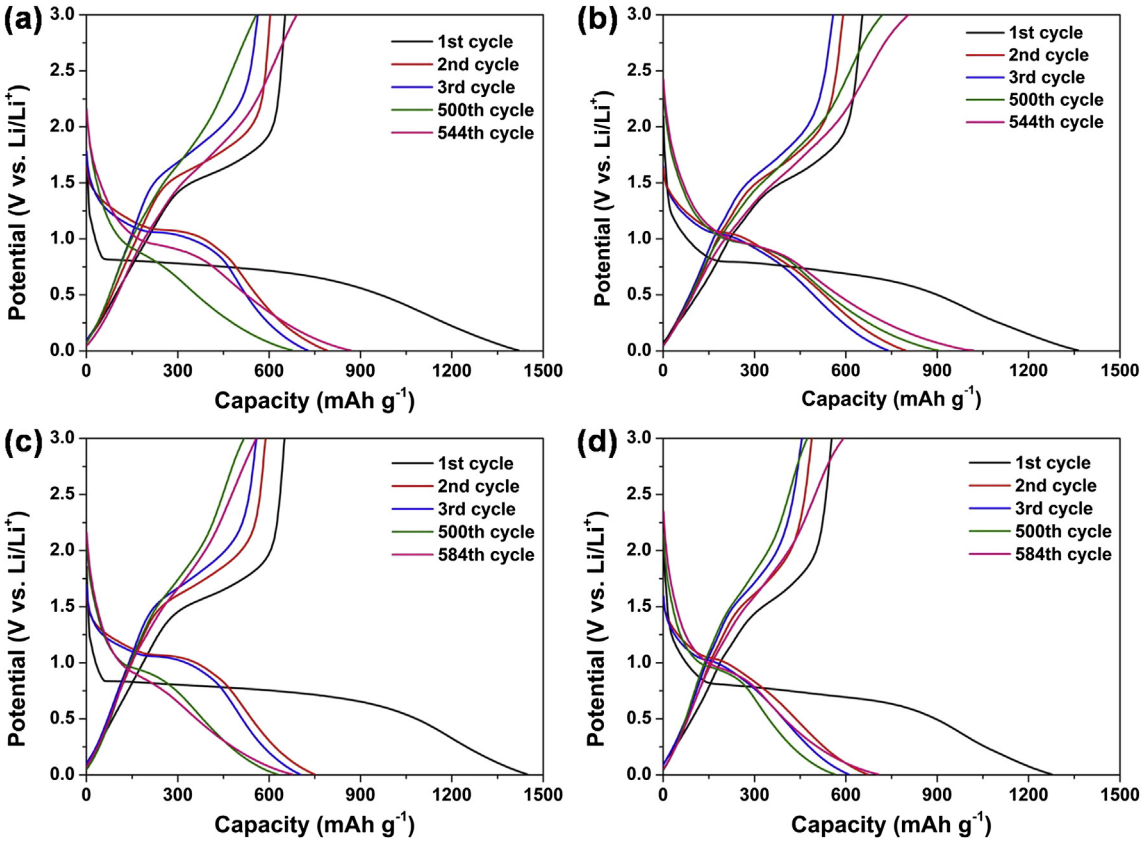

Fig. 6. Charge/discharge profiles of the (a) IOS-a, (b) IOS-b, (c) IOS-c, and (d) IOS-d electrodes at the 1st, 2nd, 3rd, 500th, and 544th or 584th cycles at a current density of 100 mA g^{-1}.

potassium-added samples demonstrated less capacity reduction due to the conversion reaction. From the results shown in Figs. 1 and 2, it was confirmed that the potassium-added IOSs contained lamellar-structured $KFeO_2$ (040) crystals. These crystals do not participate in the conversion reactions between Fe^{2+}/Fe^{3+} ions and Fe^0. Rather, they involve intercalation/deintercalation of lithium ions at a low voltage around 0 V, as shown in the CV profiles in Fig. 4. In addition, potassium addition results in smaller IOS particles, as seen in Figs. 1 and 2, and the conversion reaction initiates at a relatively higher discharge capacities in the potassium-added samples (150 mAh g^{-1}) than in the samples without potassium (60 mAh g^{-1}). It was previously observed by Larcher et al. [21] that nano-sized Fe_2O_3 with diameters of 20 nm maintained a corundum structure for up to approximately 150 mAh g^{-1} during the reduction process, whereas micro-sized Fe_2O_3 with a mean diameter of 0.5 μm underwent an irreversible structural change by the conversion reactions as soon as the discharge capacity reached 10 mAh g^{-1}. Thus, it can be concluded that the addition of

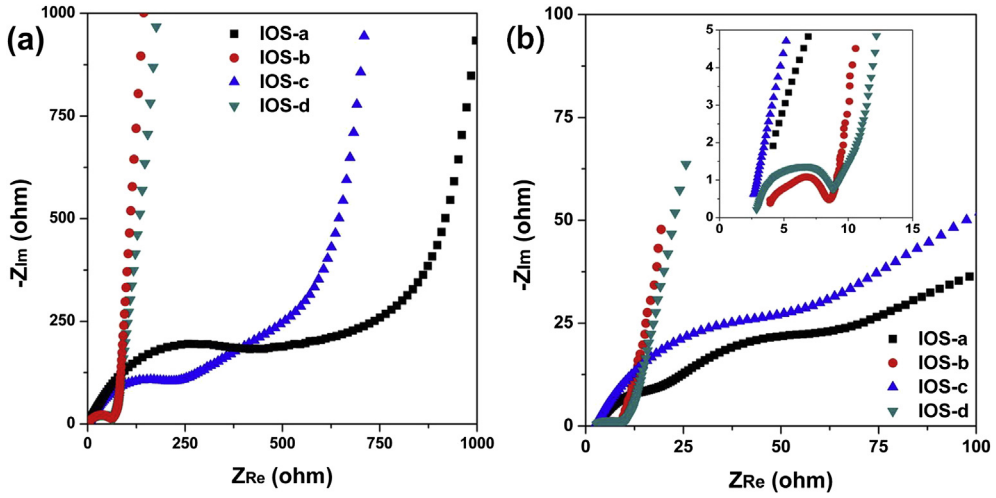

Fig. 7. Electrochemical impedance spectra of the (a) fresh and (b) extensively cycled electrodes (544 cycles for IOS-a and IOS-b, 584 cycles for IOS-c and IOS-d) shown in Fig. 5(a).

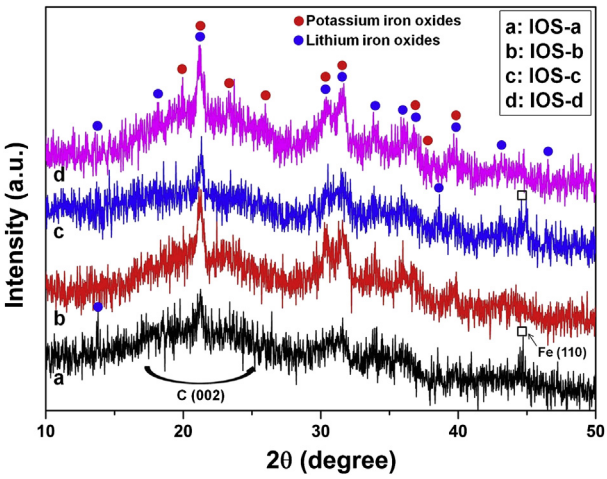

Fig. 8. XRD spectra of the IOS samples cycled more than 300 times at a current density of 1 A g^{-1}. The IOS samples were acquired by disassembling coin cells in a lithiated state.

potassium helps IOSs maintain their original structures during the beginning of lithium-ion insertion.

As can be seen in Fig. 6, the length of the plateau became shorter with increasing cycle number, whereas the remaining curve having a smooth slope became longer. In fact, the capacity in the smooth slope region is attributed to the formation of a gel-like polymeric film, as mentioned previously [17,21]. In the first tens of charge/discharge cycles, the highly irreversible conversion reactions are dominant and thus, the capacity decreases. Meanwhile, as the number of cycles increased, the growth of the polymeric film due to reactions between the electrolyte and lithium with iron as a catalyst resulted in a gradual increase of capacity, as displayed in Fig. 5. In comparison with the samples without potassium addition, the smooth curves in the potassium-added electrodes became longer, indicating that the potassium addition makes the formation of the polymeric film easier. This result is likely due to enhancement of the electric conduction with the aid of potassium doping so that on the surface of metallic iron, the charge transfer between lithium and carbonate electrolytes can occur more easily. It should also be noted that the potassium-added samples show more tailed voltage profiles around 0 V in Fig. 6. Combined with the CV results shown in Fig. 4, this demonstrates that potassium addition contributes to maintaining the lamellar structures of IOSs participating in highly reversible intercalation/deintercalation during repeated cycling. This is one reason why the potassium-added samples showed a slightly higher capacity after long-term use than the samples without potassium addition.

To clearly investigate the effect of potassium doping on cell resistance, the electrochemical impedance spectra of fresh electrodes and extensively cycled electrodes (544 cycles for IOS-a and IOS-b, and 584 cycles for IOS-c and IOS-d) were examined, and the results are presented in Fig. 7. Based on the size of the semicircles in the medium frequency region, the charge transfer resistances of the potassium-added samples are remarkably low compared to those

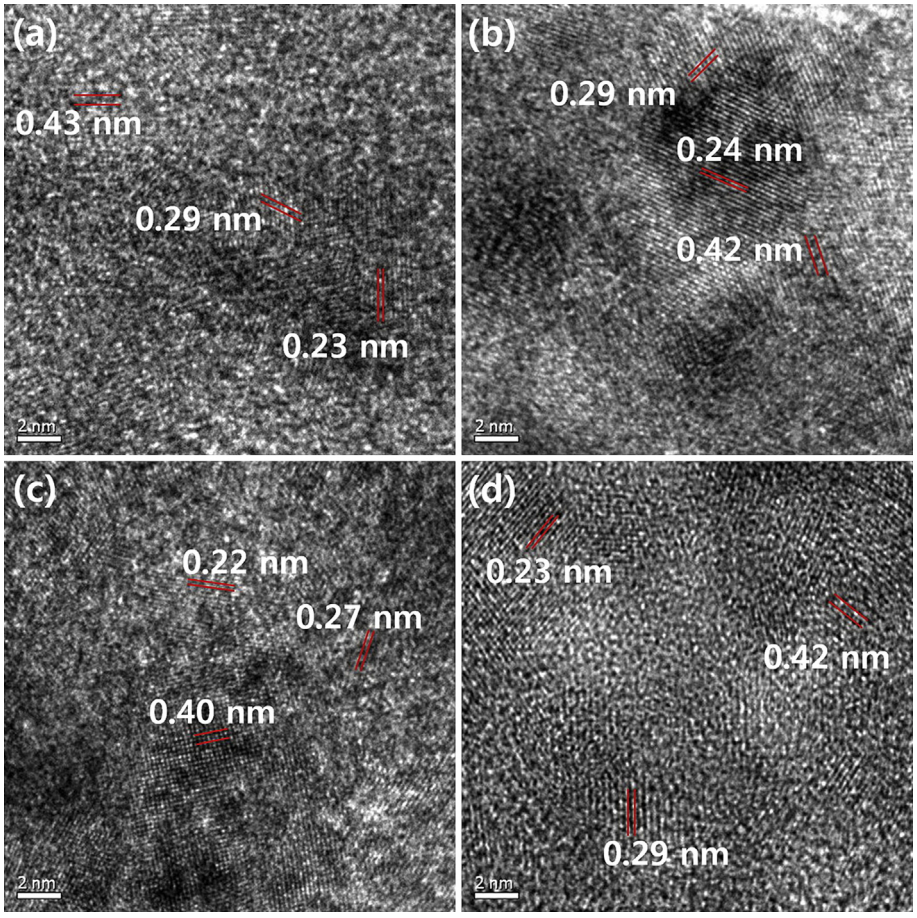

Fig. 9. TEM images of the (a) IOS-a, (b) IOS-b, (c) IOS-c, and (d) IOS-d samples cycled more than 300 times at a current density of 1 A g^{-1}. The IOS samples were acquired by disassembling coin cells in a lithiated state.

of the samples without potassium addition (IOS-a and IOS-c electrodes). On the other hand, the sheet resistances of the fresh IOS electrodes measured by a resistance tester (CMT-100M, AIT. Co.) were nearly identical, with values in the range of 2.2–2.4 mΩ sq^{-1}. The rate of the charge transfer reactions at an interface is determined by the rate of electron jumping across the interface in the electric double layer as well as the electronic conduction in the electrode. Of course, the rate of reactions can also be limited by lithium-ion transfer in the electrolyte, which is expressed as the Warburg resistance in the relatively low frequency region of the EIS. Therefore, the addition of potassium into iron oxides can help electrons jump across the interface between the electrode and electrolyte and reduce the charge transfer resistance. As demonstrated in the CV and EIS results in Figs. 4 and 7, this positive effect of potassium addition remains even after 500 charge/discharge cycles.

Through XRD and TEM analyses, we investigated the changes of the crystal structures resulting from extended cycling of the IOS samples (charged/discharged more than 300 cycles) shown in Fig. 5b. We used lithiated samples to observe the IOS phases when lithium is inserted into the phases.

The broad diffraction peaks in Fig. 8 at 2θ values between 15 and 25° correspond to the (002) crystalline plane of the super-P used as a conductive additive. Iron oxides (Fe_3O_4, Fe_2O_3, FeO) or $KFeO_2$ were transformed into various lithium iron oxides ($LiFeO_2$, Li_5FeO_4, and $LiFe_5O_8$ referenced in JCPDS Nos. 85-1991, 37-1151, and 13-0207) and potassium iron oxides (K_2FeO_4, $K_2Fe_{10}O_{16}$, and $KFe_{11}O_{17}$ referenced in JCPDS Nos. 83-2316, 70-1523, 40-0135, and 87-1546) over the course of lithium insertion. In particular, the XRD peaks attributed to orthorhombic Li_5FeO_4 with a *Pbca* space group (JCPDS No. 37-1151), which were similar to the structure of $KFeO_2$, occurred strongly at $2\theta = 21.1$, 30.3, and 31.6°. Their intensities were much stronger in the potassium-added IOS-b and IOS-d samples than in the samples without potassium addition (IOS-a and IOS-c). In addition, the particle sizes of the IOS-a, IOS-b, IOS-c, and IOS-d samples calculated using the Scherrer equation [11] are 2.2 nm, 3.5 nm, 2.7 nm, and 4.9 nm, respectively, which are much smaller than their respective fresh particles. This is likely due to pulverization of the material developed during the conversion reaction.

In accordance with the XRD results shown in Fig. 8, the TEM results showed that the IOS particles became smaller and their various phases were transformed to similar crystal structures with close d-spacings after long-term use. Additionally, the potassium-added samples in Fig. 9b and d showed higher crystallinities than the samples without potassium addition shown in Fig. 9a and c. Consequently, the addition of potassium helps to maintain the crystal structures of IOS even though it does not prevent material pulverization.

4. Conclusion

Iron oxide scales reproduced via the quenching of carbon steel are employed in anode materials, and the effects of potassium addition on their electrochemical performances are investigated. The potassium added to IOS forms a lamellar structure of $KFeO_2$ from Fe_2O_3 lattices in the IOS nanoparticles. The lamellar $KFeO_2$ is electrochemically active and strong, and thus retains its high crystallinity and reversible lithium storage capacity even after more than 500 charge/discharge cycles. The addition of potassium also helps to maintain good electrical contact in the IOS electrodes during cycling, leading to a significant decrease in the charge transfer resistance. Therefore, compared to the samples without the addition of potassium, the potassium-added IOSs show a higher capacity rate increase, which occurs sometimes in electrodes containing nano-sized 3d-transition metal oxides such as cobalt, nickel, or iron oxides. In conclusion, the presence of potassium in iron oxides is highly efficient in enhancing both the capacity and cycling capability of LIBs. These studies provide a simple and valuable method for reusing cheap IOSs and can be applied to iron oxides prepared by any methods other than the quenching of carbon steel.

Acknowledgements

The work was supported by the 2013 research fund of the University of Ulsan.

References

[1] J. Cabana, L. Monconduit, D. Larcher, M.R. Palacín, Adv. Mater. 22 (2010) E170–E192.
[2] J. Chen, L.N. Xu, W.Y. Li, X.L. Gou, Adv. Mater. 17 (2005) 582–586.
[3] J.S. Chen, T. Zhu, X.H. Yang, H.G. Yang, X.W. Lou, J. Am. Chem. Soc. 132 (2010) 13162–13164.
[4] W.M. Zhang, X.L. Wu, J.S. Hu, Y.G. Guo, L.J. Wan, Adv. Funct. Mater. 18 (2008) 3941–3946.
[5] J. Roederer, F. Jeannot, B. Dupré, C. Gleitzer, React. Solids 2 (1986) 245–252.
[6] M. Gougeon, B. Dupré, C. Gleitzer, Metall. Trans. B 17 (1986) 657–663.
[7] P.G. Bruce, B. Scrosati, J.M. Tarascon, Angew. Chem. Int. Ed. 47 (2008) 2930–2946.
[8] U. Kasavajjula, C. Wang, A.J. Appleby, J. Power Sources 163 (2007) 1003–1039.
[9] H. Kim, M. Seo, M.H. Park, J. Cho, Angew. Chem. Int. Ed. 49 (2010) 2146–2149.
[10] M.E. Bolster, US patent No. 5691083 (1996).
[11] D.W. Jung, J.H. Jeong, B.S. Kong, J.K. Lee, E.S. Oh, J. Nanosci, Nanotechnology 12 (2012) 3317–3321.
[12] L.H. Wu, H.B. Yao, B. Hu, S.H. Yu, Chem. Mater. 23 (2011) 3946–3952.
[13] X. Zhu, Y. Zhu, S. Murali, M.D. Stoller, R.S. Ruoff, ACS Nano 5 (2011) 3333–3338.
[14] Y. Zou, J. Kan, Y. Wang, J. Phys. Chem. C 115 (2011) 20747–20753.
[15] B. Koo, H. Xiong, M.D. Slater, V.B. Prakapenka, M. Balasubramanian, P. Podsiadlo, C.S. Johnson, T. Rajh, E.V. Shevchenko, Nano Lett. 12 (2012) 2429–2435.
[16] K.H. Kim, D.W. Jung, V.H. Pham, J.S. Chung, B.S. Kong, J.K. Lee, K. Kim, E.S. Oh, Electrochim. Acta 69 (2012) 358–363.
[17] S. Grugeon, S. Laruelle, L. Dupont, J.M. Tarascon, Solid State Sci. 5 (2003) 895–904.
[18] X.J. Zhu, Z.P. Guo, P. Zhang, G.D. Du, R. Zeng, Z.X. Chen, S. Li, H.K. Liu, J. Mater. Chem. 19 (2009) 8360–8365.
[19] G. Zhou, D.W. Wang, P.X. Hou, W. Li, N. Li, C. Liu, F. Li, H.M. Cheng, J. Mater. Chem. 22 (2012) 17942–17946.
[20] R. Gnanamuthu, C.W. Lee, Mater. Chem. Phys. 130 (2011) 831–834.
[21] D. Larcher, C. Masquelier, D. Bonnin, Y. Chabre, V. Masson, J.B. Leriche, J.M. Tarascon, J. Electrochem. Soc. 150 (2003) A133–A139.